Model validation of the ASTERIA-FBR code related to core expansion phase based on THINA experimental results

T.Ishizu[1], H.Watanabe[1]

[1] Regulatory Standard and Research Department, Secretariat of Nuclear Regulation Authority (S/NRA/R), Tokyo, Japan

E-mail contact of main author: tomoko_ishizu@nsr.go.jp

Abstract. Mechanical consequences which might be caused by core disruptive accident (CDA) are one of the major concerns in safety of fast reactors (FRs). Once a severe re-criticality occurs, the core materials are vaporized creating CDA bubbles which consists of fuel vapor, steel vapor, sodium vapor and fission gases. The high-pressured CDA bubbles expand rapidly and drive a sodium slug in the upper plenum. The upward-accelerated sodium slug compresses the cover-gas region with increase of the pressure. This pressure increase might cause to threaten the reactor vessel integrity. To evaluate the mechanical energy affecting the boundary integrity, the energy conversion from thermal energy to mechanical energy plays an important role. This paper describes model validation study of ASTERIA-FBR application to the thermal-to-mechanical energy conversion process, focusing on calculation models through the THINA test simulation. As a result, it was confirmed that the energy conversion process and its ratio were in good agreements with the experimental results. The mechanism of CDA bubble expansion and the uncertainty brought by the calculation models were also discussed.

Key Words: fuel-coolant interaction, THINA experiment, ASTERIA-FBR, energy conversion.

1. Introduction

One of major concerns for safety of sodium cooled fast reactors is that the cores are not designed in their maximum reactive configuration. This characteristic causes the increase of probability to exceed super-prompt criticality during the core disruptive accident (CDA). Once the severe re-criticality occurs due to the change of core configuration, the core materials are vaporized creating CDA bubbles and the bubbles expand in a very short time. The expansion of CDA bubble drives the sodium slug in the upper plenum providing mechanical energy resulting in threatening the reactor vessel integrity. Thus, it is important to simulate the core expansion phase and to calculate precisely the released mechanical energy.

For the purpose of evaluating the released mechanical energy during CDA, S/NRA/R (including ex-JNES) has been developing an ASTERIA-FBR code [1, 2]. ASTERIA-FBR is a CDA calculation code for sodium-cooled fast reactors. The event of special interest for the code development is Unprotected-Loss-Of-Flow (ULOF). ASTERIA-FBR can be applied to the several phases during ULOF event such as initiating phase (IP), transition phase (TP), and post disassembly expansion phase (PDE), and a part of post-accident material relocation phase (PAMR) and post-accident heat removal phase (PAHR). In this code development, the models to calculate fuel-coolant interaction (FCI) and the related phenomena which occur in the upper sodium plenum of reactor vessel have been validated based on THINA experimental results [3].

In this paper, overview of ASTERIA-FBR is summarized in Section 2, and the outline of THINA experiment and its simulation using ASTERIA-FBR are explained in Section 3. Finally the parametric study regarding the interfacial area is discussed in Section 4.

2. Overview of ASTERIA-FBR

2.1.Code structure

Figure 1 shows the code structure of ASTERIA-FBR. ASTERIA-FBR consists of three major modules; a thermo-fluid dynamics calculation module, CONCORD [4], a fuel behavior calculation module, FEMAXI-FBR [5], and a space-time neutronics calculation module, PARTISN/RKIN. The data transfer in each time-step is conducted between these modules via ASTERIA-CNTL which deals with not only performing data transfer but also collecting the major calculation results from all modules and sends to the next time step for each module. The thermo-fluid dynamics calculation module was used for the simulation of THINA experiment. In the following section the outline of CONCORD is described in more detail.

2.2.Thermo-fluid dynamics calculation module: CONCORD

CONCORD is a three-dimensional, multi-velocity field, multi-phase, multi-component, and Eulerian fluid dynamics code as shown in Fig. 2. Mass conservation equation, momentum conservation equation and energy conservation equation are used to calculate each component in the liquid field and gaseous field. CONCORD is characterized from being a three- or two-dimensional calculation system and installation of equation-of-state, interfacial area, and phase change such as vaporization/condensation and melting/freezing. The calculation scheme consists of three steps; first, the fluid-dynamics for mass, internal energy, and momentum of each component are calculated for the prediction (STEP-A), second, the pressure balance is calculated (STEP-B), and finally the fluid-dynamics are obtained with no contradiction results (STEP-C). The specific features of major models in CONCORD are described as follows:

(1) Multi-velocity-field, multi-phase, multi-component

The multi-component model in a cell is schematically summarized in Fig. 2(1). For the structure field, 3 material components are prepared; pin element, steel structure, and mixture crust. For the liquid field, 7 energy components are prepared; liquid fuel, fuel particles, fuel chunks, liquid steel, steel particles, control material, and liquid sodium. For the gaseous field, 8 material components are prepared; fuel vapor, steel vapor, sodium vapor, fission product gas, nitrogen, oxygen, argon, and helium. In the calculation, 3 phases of solid, liquid, and gas can be considered separately.

(2) Energy exchange model

The heat transfer among structure-field components, liquid-field components, and vapor-field components is calculated by multiplying the temperature difference between the interacting components by the heat-transfer coefficient and contact surface area. Heat transfer coefficients are derived from the interaction equation between the set of materials and/or conditions based on the flow regime and the binary contact area.

The convective interfacial area model was developed based on the interfacial area concentration mechanism proposed by Ishii [6]. And the convection model of the number density of bubbles by Kocamustafaogullari and Ishii [7] was used. The fundamental equation of the model is expressed as follows:

$$\frac{\partial A}{\partial t} + \nabla \cdot (v\mathrm{A}) = \sum_k S_k \qquad \ldots.(1)$$

where A refers to the interfacial area concentration of dispersed particles (bubbles and droplets), v refers to the convective velocity, and S_k indicates to be the source term. The source term S_k is evaluated taking account of bubble nucleation, coalescence of bubbles and droplets, Weber number breakup, turbulence breakup, flashing and mass transfer. The interfacial area plays a key role to the heat transfer and momentum exchange. In the convection flow, the interfacial area is calculated using the droplets/particles size based on Weber number.

The heat transfer is calculated by using interfacial concentration model with three velocity fields model. Pool flow regime model is implemented taking account of void fraction in a cell as shown in Fig. 2(2). In addition, delayed neutron precursor is taken into account as one of the materials to evaluate the transport to primary coolant system including the cover-gas region.

(3) Momentum exchange model

Momentum exchange between the components is brought by the drag forces and mass exchange. The momentum exchange due to the drag forces is calculated by the momentum exchange function which is derived from friction among the interacting components.

(4) Mass exchange model

Mass exchange is calculated based on the phase change among solid, liquid, and vapor. Figure 2(3) shows the phase change paths for vaporization/condensation (V/C) which are implemented in CONCORD. A number of heat transfer paths for vaporization/condensation and for melting/freezing are prepared in the phase change model.

3. THINA experimental analysis

3.1. Review of TH564 test

The THINA out-of-pile test series [5] have been carried out using THINA facilities located in the KfK (current KIT) in Germany. The objectives of the experiments were to investigate the phenomenology and physics of FCI with melt in the sodium pool. Table I summarizes the experimental condition of TH564 test in the THINA experimental series.

TABLE I: INITIAL CONDITION OF TH564 TEST.

		TH564
Melt	Composition	24 w/o Al_2O_3+76 w/o Fe
	Mass (kg)	5.5
	Temperature (K)	3,270
	Driving force (at the bottom of pool) (MPa)	2.5
	Injecting duration (ms)	136
Coolant	Composition	Na
	Mass (kg)	155
	Coolant level (m)	2.70
	Temperature (K)	763≈795
	Subcool temperature (K)	≈380
	Pool radius (m)	0.3
Cover-gas	Pressure (MPa)	0.11
	Volume (m^3)	0.15

The facility consisted with a cylindrical sodium pool with 0.15 m in radius and 5.0 m in height (2.7 m for sodium pool and 2.3 m for cover-gas region), thermite melt injector, slide valves and a set of measurement equipments: pressure transducers, level indicators, temperature and void sensors and an x-ray tube and a high speed camera. The sodium pool was filled with sodium of 155 kg at 770 K, and the cover-gas area was filled with argon gas of 0.11 MPa.

The test was initiated by the melt injection of 5.5 kg which consists of iron with 76 wt.% and alumina (Aluminum oxide) with 24 wt.% at 3270 K. The melt injection to the sodium pool was driven by non-condensable gas with the pressure of 2.5 MPa. The injecting duration time was measured to be 136 ms. The melt contacted with the sodium with intense heat transfer immediately generated the sodium vapor in the vicinity of the melt. A large two-phase region filled with sodium vapor expanded with driving the sodium slug in the upper plenum and raising up the sodium level of the pool. The sodium level rise compressed the cover-gas region and increased the cover-gas pressure. After the cover-gas pressure peak, the sodium level went down and the two-phase region turned to be condensed. In this test, transients of pool pressure, cover-gas pressure, expansion of two-phase region, and change of sodium level were measured. Based on the reference [5], the mechanical work was calculated to be 26 kJ using the following formula:

$$E_{mech} = \int_{t=0}^{t_e} P_1(t)dV \qquad \text{.....(2)}$$

where $P_1(t)$ is the time history of the pressure signal of sodium pool bottom (z=100 mm), $dV(=Adz_l)$ is the change in the two-phase volume, t_e is the time when the vapor volume is the maximum, A is the vessel cross-section, and $z_l=f(t)$ is the time history of change of the sodium level.

Taking account of the initial internal energy (E_{th}) of the melt to be 12500 kJ, the energy conversion ratio which is calculated by mechanical energy E_{mech} divided by E_{th} was evaluated to be 0.21 %.

3.2. Calculation condition

The calculation system of ASTERIA-FBR is shown in Fig 3. Since the experimental system was a cylindrical shape, the two-dimensional system (R-Z) with 6x33 calculation cells was applied. The melt was assumed as a mixture component of iron and alumina. Thus, 4 material components of alumina, iron, sodium, and argon gas were considered in this analysis. The phase change of each component was calculated based on their own EOSs. Since the number of velocity fields is limited to be three, however, the heat transfer and momentum exchange of melt were calculated based on the same velocity, that is, without distinction between alumina and iron in the melt.

The melt was injected with the inlet pressure of 2.5 MPa to the sodium pool with bottled-up condition. The injected melt was assumed to contain 10 % mass of non-condensable gas in the melt [8]. The pressure drop coefficient at the melt inlet was set to be 4.5 based on the preliminary calculation results assuming that 5.5 kg of melt was injected in the duration time of 136 ms under the condition of inlet pressure of 2.5 MPa. A throttle plate mounted at the location of 2.0 m high from the pool bottom was modeled as a fluid resistance with reduction of flow cross section to 33 % by setting structure of each horizontal side of the calculation cells at Z=2000 mm and with pressure drop coefficient of 3.0.

3.3. Calculation results (Base case)

Calculation results are shown in Figs. 4(1) to (5) compared with the experimental results. Figure 4(1) and (2) indicate transients of pool pressure and cover-gas pressure, respectively. Figure 4(3) shows the transients of void and sodium region with the sodium level and growth/collapse of two-phase region of the test result. Figure 4(4) shows the snapshots of the void and sodium volume fractions with the measured change of two-phase region in the test.

When the melt jet injected into the sodium pool, sodium vaporized and condensed intermittently by contact with the melt. CONCORD could simulate the pool pressure oscillation due to FCI although the pressure peaks were underestimated a little (Fig. 4(1)). A two-phase region was created and expanded in the pool (Fig. 4(3), and (4)). Rapid expansion of the two-phase region drove the sodium slug upward compressing the cover-gas region.

CONCORD could simulate the expansion by simulating the heat transfer from the melt to sodium at the front edge of the region and generating the sodium vapor. The flow regimes was calculated to be a dispersed flow regime inside the two-phase region, a transition flow regime at the boundary of the region, and the bubbly flow regime in the pool. This indicates that the heat transfer governed by contact condition at the boundary of the two-phase region is important for the subsequent expansion.

Due to the compression of cover-gas region by the accelerated sodium slug, the cover-gas pressure reached to approximately 0.19 MPa at the maximum (vs. 0.24 MPa in the test) (Fig. 4(2)). After the cover-gas pressure peak, the pool pressure temporally settled from t=0.2 s to 0.5 s. This is due to the decrease in the contact area between melt and sodium by expansion of the two-phase region (Fig. 4(1)). When the sodium vapor in the two-phase region condensed, the contact area between the melt and the liquid sodium increased again and a pressure pulse of the pool appeared at 0.53 s (vs. 0.6 s in the test). This transient of the calculated sodium volume fraction at the upper boundary showed to be consistent with the pressure transient of the sodium pool and the cover-gas region (Fig. 4(3)).

Mechanical energy was calculated by integration of volume change of two-phase region and the pressure transient based on the equation (2). The result is shown in Fig. 4(5). The increase rate of the energy of the calculation result was the same as the test result, and the peak energy of 22 kJ was a little less than the test result of 26 kJ. The energy conversion ratio was calculated to be 0.176 % against 0.21 % of the test result.

It can be concluded that CONCORD reasonably reproduces the phenomena in good agreement. The margin of error in the mechanical energy was evaluated to be 15%.

4. Parametric study on particle size

In this section, parametric study and the discussion are made on the heat transfer and fluid dynamics of the phenomena focusing uncertainties in the interfacial area.

Interfacial area (IFA) among the liquid material components is important for both the heat transfer and the momentum exchange. The radii of fluid components (droplets, particles, chunks, and bubbles) were set to be 0.05 mm to 10 mm in the base case. Radius sizes of the fluid components in convection flow are calculated automatically in the range of radius taking account of the Weber number. In this study, parametric calculation was performed with changing IFA, that is, adopting the comparable extent of particle radius with the experimental results. The radii of particles were unclear at the timing of phase change in the test. The report of post-test examination, however, showed the evaluated main distribution range of particle radii of 0.016 mm to 1 mm, and mentioned that and about 90 % of weight of the fragments

was less than 1mm in diameter and about 40-50% less than 0.25 mm. In this study, three parametric calculations were conducted with setting the particle radii with the range of 0.016 mm to 2, 5, and 10 mm, respectively. Calculation results of pool pressure and mechanical energy are shown in Figs. 5(1) and (2) compared with the experimental results and the base case. The initial oscillation of pool pressure was approximately reproduced until the melt injection ends at t=0.136 s although the oscillation durations were a little longer than those of the experimental result and base case. It was found that decrease of minimum size of particles leads to faster expansion of two-phase region. Since the mechanical energy is evaluated based on transient of pool pressure and volume of two-phase region as mentioned in Sec.3.1, the mechanical energy of parametric cases were evaluated to be larger than base case.

After the two-phase region is developed at about t=0.2 s, the pool pressure of the parametric cases remains 0.1-0.2 MPa higher than the experimental result. This result indicates that the heat exchange between the melt and sodium is too large in the particle size modelling to condense the two-phase region in the calculation. Taking into account the result of post-test examination that most particles are less than 1 mm in radius, it is considered that the rest several percents of particles plays a key role for the condensation in the later process. That is, smaller particles were generated in the early phase, and larger particles were created in the later phase during the melt injection. Since the two-phase region was already developed in the later phase, it was presumed that FCI was not significant enough to cause fragmentation. This estimation is reasonable based on the intensity of FCI and resultant relative velocity between melt and sodium.

Due to the inability of simulating these fragmentation processes precisely with Eulerian fluid dynamics codes and as considered the pressure transient of base case is closer to the experimental result compared with parametric cases with set of the range of particles, it is preferable that the particle size range of the base case should be employed.

5. CONCLUSIONS

As a part of model validation study of ASTERIA-FBR, a simulation against TH564 test in THINA experimental series was performed using CONCORD, a thermo-fluid dynamics module of ASTERIA-FBR.

The calculation result of CONCORD reasonably reproduced the experimental transient such as pool pressure increase due to FCI after the melt injection, the cover-gas compression caused by the upward-accelerated sodium slug, and the pool pressure pulse due to condensation of two-phase region. The mechanical energy was evaluated to be 22 kJ which is the error margin of 15% compared with the test result. Although expansion of the calculated two-phase region was underestimated compared with the test result especially in the later phase, it can be concluded that CONCORD simulates the phenomena which occurred in the test with in good agreement.

Based on the parametric study with changing particle size, it was confirmed that interfacial area plays a key role for the expansion/condensation of the two-phase region. The base case was compared with the parametric case taking account of the particle sizes measured in the post-test examination of TH564. As a result, the base case could simulate the test result better than the parametric cases in the case of FCI triggered by melt injection into the sodium pool.

In the future, further model validation studies of ASTERIA-FBR are planned focusing on the phenomena with heat transfer and can-wall structure failure by simulation of in-pile and out-of-pile experiments.

ACKNOWLEDGEMENTS

The author would like to express her gratitude to Yuichi Yamamoto of Japan Systems Corp., and Noriyuki Shirakawa of The Interactions Research Inc. for their large contribution to the calculating works.

References

[1] ISHIZU, T., ENDO, H., TATEWAKI, I., YAMAMOTO, T., SHIRAKAWA, N., " Development of Integrated Core Disruptive Accident Analysis Code for FBR - ASTERIA-FBR," Proceedings of ICAPP '12, Chicago, USA, June 24-28, (2012) Paper 12100.

[2] ISHIZU, T., ENDO, H., YAMAMOTO, T., TATEWAKI, I., "Core Disruptive Accident Analysis using ASTERIA-FBR," Joint International Conference on Supercomputing in Nuclear Applications and Monte Carlo 2013 (SNA+MC 2013), La Cité des Sciences et de l'Industrie, Paris, France, October 27-31, (2013).

[3] HUBER, F., KAISER, A., and PEPPLER, W., "Experiments on the Behaviour of Thermite Melt Injected into Sodium ‑Final Report on the THINA Tests Results," Proceedings of IAEA/IWGFR Technical Committee Meeting on Material-Coolant Interactions and Material Movement and Relocation in Liquid Metal Fast Reactors, 167-198, Oarai, Japan, (1994)

[4] YAMAMOTO, Y., SHIRAKAWA, N., ISHIZU, T., ENDO, H., " Development of Integrated Core Disruptive Accident Analysis Code, ASTERIA-FBR (2) Model overview and code validation of thermo-fluid dynamics module," Proceedings of Annual meeting of Atomic Energy Society of Japan, Tokyo, Japan, (2014) [in Japanese]

[5] OKAWA, T., TSUBOI, Y., SAITOU, H., TATEWAKI, I., ISHIZU, T., ENDO, H., "Fuel Behavior Simulation Code FEMAXI-FBR Development for SFR Core Disruptive Accident Analysis," Proceedings of FR'13, Paris, France, (2013)

[6] ISHII, M., *Thermo-fluid Dynamics Theory of Two-phase Flow*, Eyrolles, Paris (1975)..

[7] KOCAMUSTAFAOGULLARI, G., and ISHII, M., "Interfacial Area Nucleation Site Density in Boiling Systems," Int. J. Heat Mass Transfer, 26, No.9, 1377-1387, (1983).

[8] MORITA, K., KONDO, Sa., TOBITA, Y., BREAR, D.J., "SIMMER-III applications to fuel-coolant interactions," Nuclear. Engineering and Design, 189, pp.337-357, (1999)

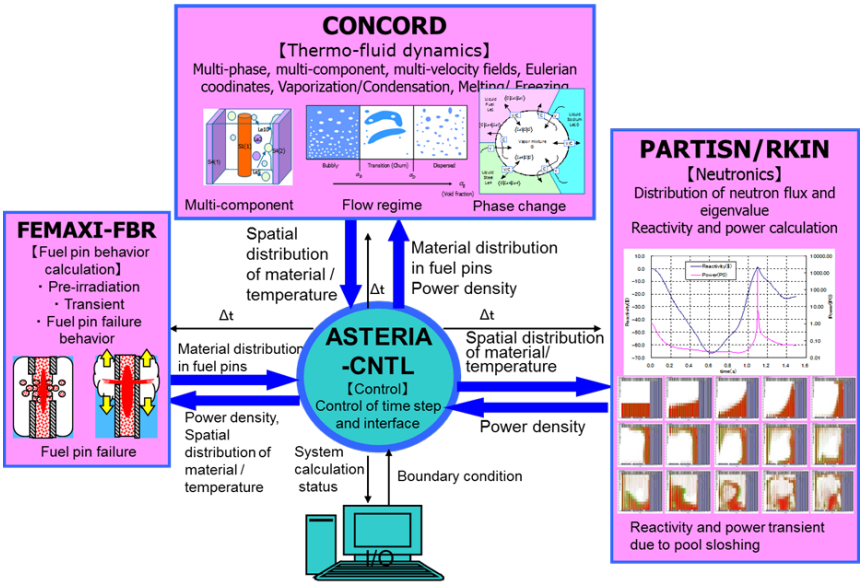

FIG. 1. Code structure of ASTERIA-FBR

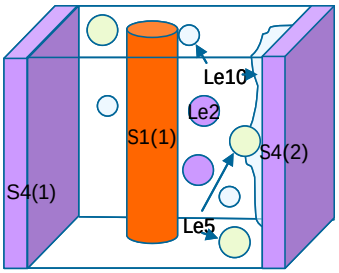

(1) Multi-component model

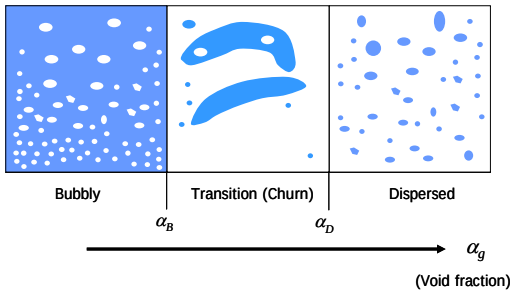

(2) Pool flow regime model

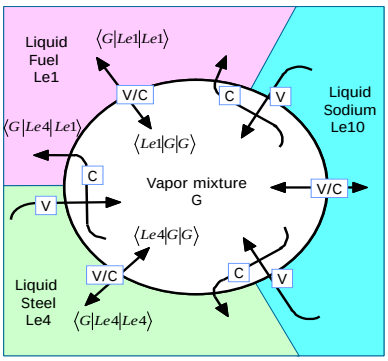

(3) Phase change model

FIG. 2. Major models of CONCORD

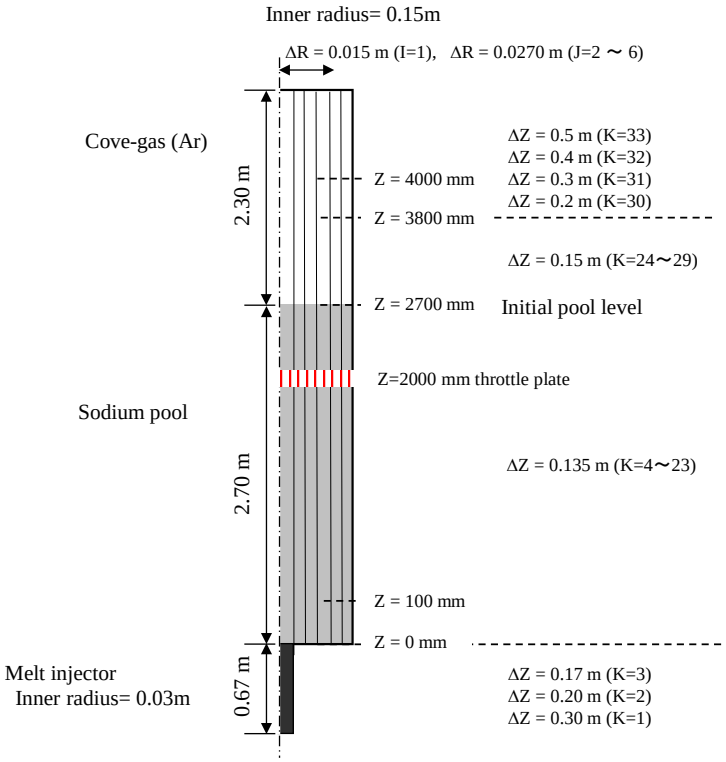

FIG.3. Calculation system

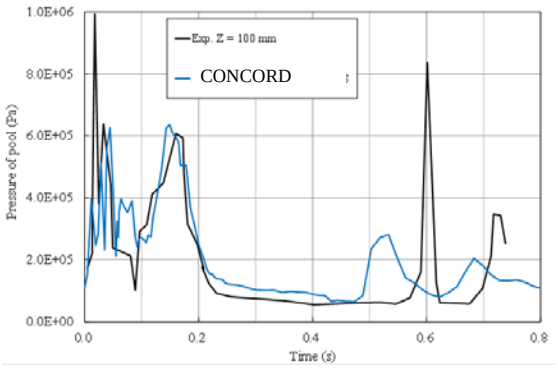

FIG. 4(1). Pool pressure at Z=100mm (Base case)

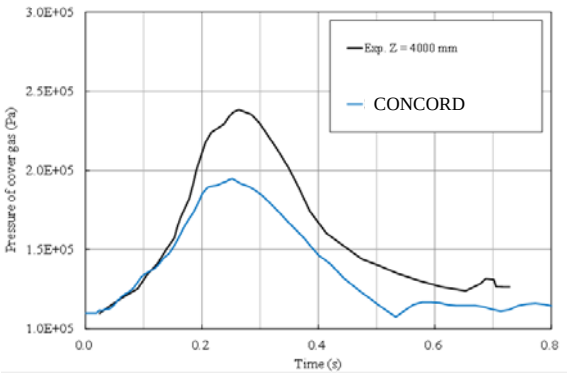

FIG.4(2). Cover-gas pressure at Z=4000mm (Base case)

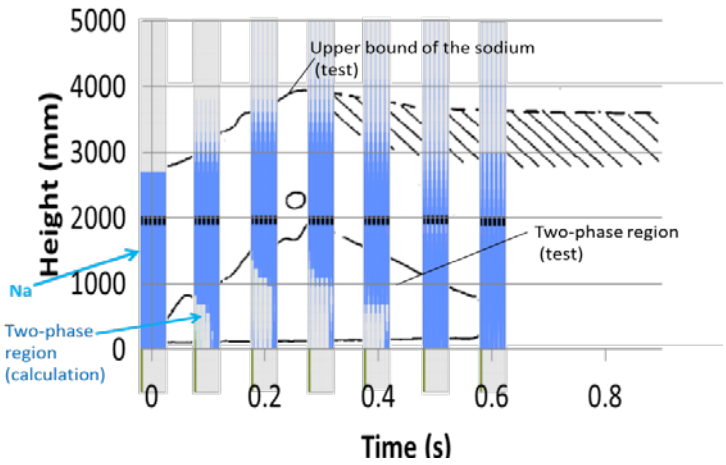

FIG.4 (3). Expansion of two-phase region (Base case)

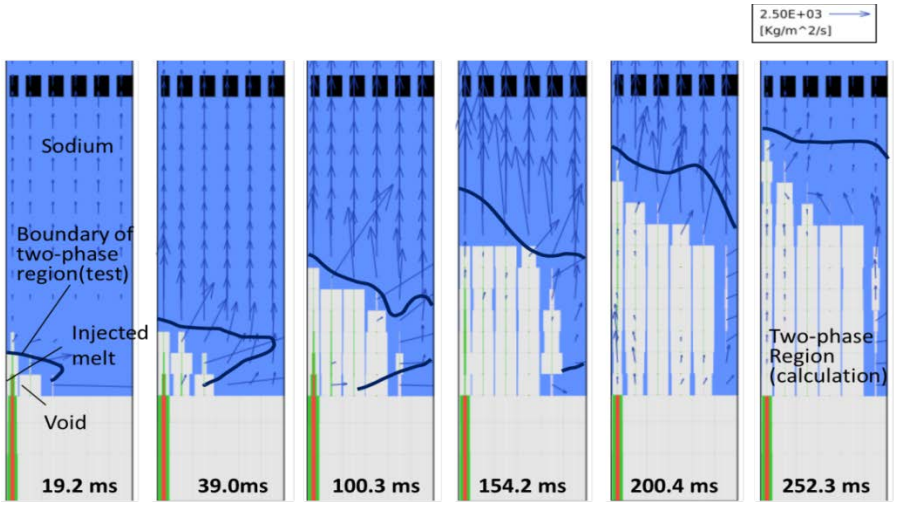

FIG.4 (4) Distribution of volume fraction in the pool (Base case)

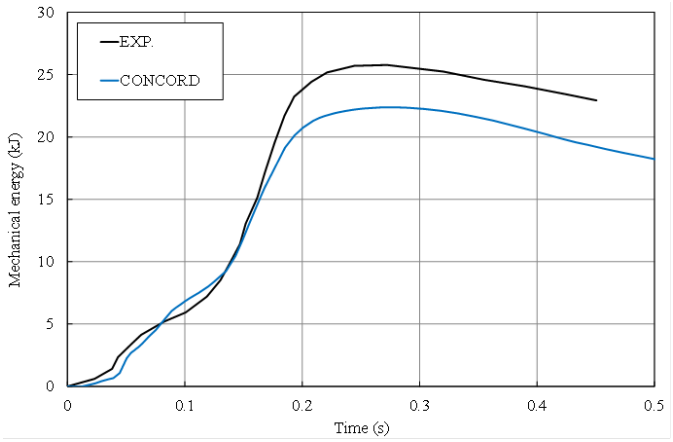

FIG.4(5). Mechanical energy (Base case)

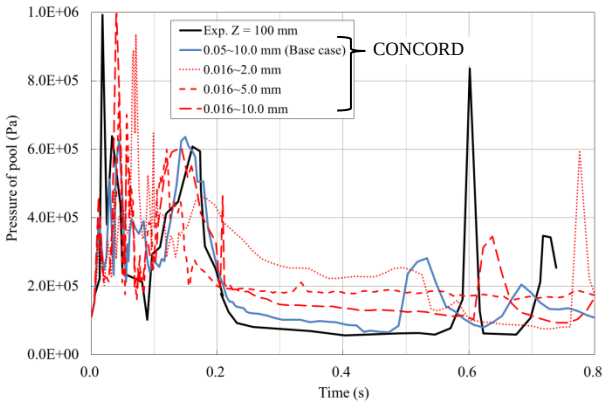

FIG. 5 (1). Pool pressure transient (Parametric case)

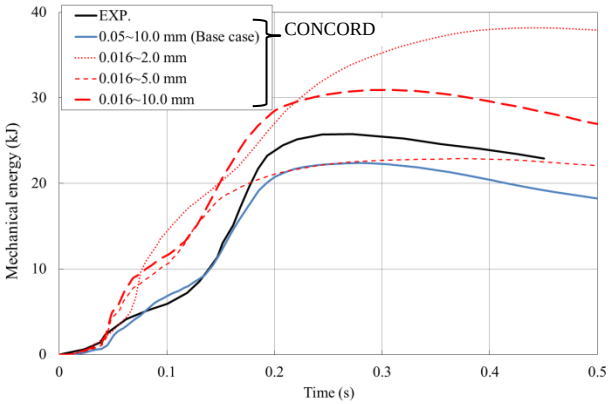

FIG. 5(2). Mechanical energy (Parametric case)